This is the peer-reviewed, final accepted version for American Mineralogist, published by the Mineralogical Society of America.
The published version is subject to change. Cite as Authors (Year) Title. American Mineralogist, in press.
DOI: https://doi.org/10.2138/am-2022-8337. http://www.minsocam.org/

Revision 1

Calorimetric study of skutterudite ($CoAs_{2.92}$) and heazlewoodite (Ni_3S_2)

JURAJ MAJZLAN[1,*], STEFAN KIEFER[1], KRISTINA LILOVA[2], TAMILARASAN SUBRAMANI[2], ALEXANDRA NAVROTSKY[2], MAREK TUHÝ[3,4], ANNA VYMAZALOVÁ[3], DMITRIY A. CHAREEV[5,6,7], EDGAR DACHS[8], ARTUR BENISEK[8]

[1] Institute of Geosciences, Friedrich-Schiller University, Burgweg 11, 07749 Jena, Germany
*corresponding author, email: Juraj.Majzlan@uni-jena.de; ORCID: 0000-0002-9151-4394
[2] School of Molecular Sciences and Center for Materials of the Universe, Arizona State University, Tempe, Arizona 85287, USA
[3] Czech Geological Survey, Geologická 6, 152 00 Prague 5, Czech Republic
[4] Institute of Geochemistry, Mineralogy and Mineral Resources, Faculty of Science, Charles University, Albertov 6, 128 00 Prague
[5] Institute of Experimental Mineralogy (IEM RAS), 142432 Chernogolovka, Moscow Region, Russia
[6] Ural Federal University, Ekaterinburg 620002, Russia
[7] Dubna State University, Dubna 141982 Russia
[8] Department of Chemistry and Physics of Materials, University of Salzburg, Jakob-Haringer-Strasse 2a, 5020 Salzburg, Austria

ABSTRACT – Nickel and cobalt arsenides, sulfarsenides, and sulfides occur in many hydrothermal ore deposits but the thermodynamic properties of these phases are not well known, in some cases not known at all. In this work, we determined a full set of thermodynamic properties for heazlewoodite and skutterudite. Both phases were synthesized in evacuated silica tubes at elevated temperatures and electron microprobe analyses gave their composition as Ni_3S_2 and $CoAs_{2.92}$, respectively. Enthalpies of formation were measured by high-temperature oxide-melt solution calorimetry. The reference phases were pure elements, thus eliminating any systematic errors related to such phases. The enthalpies of formation at $T = 298.15$ K and $P = 10^5$ Pa are –216.0±8.4(2σ) and –88.2±6.1 kJ·mol^{-1} for Ni_3S_2 and $CoAs_{2.92}$, respectively. Entropies were calculated from low-temperature heat capacity (C_p) data from relaxation (PPMS) calorimetry and are 133.8±1.6 and 106.4±1.3 J·mol^{-1}·K^{-1}, respectively. The calculated Gibbs free energies of formation are –210.0±8.4 and –79.9±6.2 kJ·mol^{-1} for Ni_3S_2 and $CoAs_{2.92}$, respectively. The PPMS C_p data, together with a set of differential scanning calorimetry

measurements, were used to derive C_p polynomials up to 700 K with the Kieffer model based on previously published frequencies of acoustic and optic modes. Equilibrium constants for selected reactions with an aqueous phase were calculated up to 700 K. Geochemical modeling in these systems, however, should await until more reliable data for other phases from the system Co-Ni-As-S are available.

Keywords: heazlewoodite; skutterudite; enthalpy; entropy; geochemical modeling

Submitted: American Mineralogist

INTRODUCTION

Nickel and cobalt arsenides, sulfarsenides, and sulfides occur in many hydrothermal ore deposits (Dolansky 2007, Belkin et al. 2008, Ahmed et al. 2009, Gervilla et al. 2012, Kreissl et al. 2018, Scharrer et al. 2019, Tourneur et al. 2021, Horn et al. 2021). They are found especially in orthomagmatic Cu-Ni-PGE ores (Naldrett 2004), hydrothermal ores, commonly of the "five-element association" (Burisch et al. 2017), or in stratiform Cu-Co ores (Dewaele et al. 2006). They represent a large and complex group of minerals, with sulfides, disulfides, mono-, di- and triarsenides, and sulfarsenides (a list of the minerals with further references can be found in Table 1 in Hem 2006). In addition to Co, Ni, and As, many of these minerals show also the As-Sb substitution, for example in the gersdorffite-ullmanite (NiAsS-NiSbS) series (Števko a Sejkora 2020). Occasionally, minerals like gersdorffite may contain economically interesting concentrations of gold or platinum-group elements (e.g., Pašava et al. 2013, Cabri et al. 2017). The presence of reduced arsenic is likely to drive gold incorporation in the sulfarsenide minerals (Pokrovski et al. 2021). Arsenides also commonly form in serpentinization processes at high T-P in subduction zones and may be important carriers of As and PGE in such settings (Gonzáles-Jiménez et al. 2021). Some of the compositions show polymorphism, for example, $NiAs_2$ is known as the minerals rammelsbergite, pararammelsbergite, and krutovite. Structural variations are encountered even within one mineral species; gersdorffite, for example, can have an ordered structure (space group $P2_13$) or two disordered structures (space groups $Pa3$ and $P1$) (Bayliss and Stephenson 1967, 1968, Steger et al. 1974, Bayliss, 1982).

Experimental work on dry systems (Klemm, 1965; Maurel and Picot, 1974, Hem and Makovicky 2004a, b, see also Table 2 in Hem 2006) showed that complete solid solutions can be

63 expected at temperatures above 500 °C but such high temperatures were rarely encountered
64 during the formation of the ores with Co-Ni arsenides and sulfarsenides (Scharrer et al. 2019).
65 Thermodynamic properties of the Co-Ni-As-S phases are mostly not well constrained or
66 unknown. For the obvious reason of their abundance, more attention was paid to the Fe-dominant
67 members of arsenides and sulfides. For example, thermodynamic properties of löllingite ($FeAs_2$)
68 were determined early by Barton (1969) from high-temperature equilibria and extrapolation to
69 room temperature. A calorimetric measurement of heat capacity (C_p) of a synthetic löllingite
70 sample and the resulting entropy by Panishkin et al. (1991) deviated much from the datum in
71 Barton (1969). In their compilation, Robie and Hemingway (1995) adopted the S^o from
72 Panishkin et al. (1991). They also selected Δ_fG^o which is numerically equal to Δ_fH^o in Barton
73 (1969) and adjusted their Δ_fH^o accordingly. The reasons behind this adjustment are not clear.
74 Bessinger and Apps (2005) modified the Δ_fG^o from Barton (1969) slightly and took S^o from
75 Barton (1969), even though they referred to Pokrovski et al. (1996) as their data source. Perfetti
76 et al. (2008) accepted S^o from Panishkin et al. (1991) and recalculated Δ_fH^o and Δ_fG^o, based on
77 their new solubility data and combustion calorimetry data of Stolyarova (1977). When reviewing
78 the available source of thermodynamic data for löllingite, one notes differences of 40 $kJ \cdot mol^{-1}$ in
79 Δ_fH^o and 40 $J \cdot mol^{-1} \cdot K^{-1}$ in S^o (see also Perfetti et al. 2008). Such differences are larger than
80 expected experimental uncertainties in thermodynamic measurements. This example shows the
81 difficulties and gaps in our understanding of these minerals, even though the Fe-As-S system
82 received much more attention than the systems Co-As-S or Ni-As-S.
83 In this work, we have derived thermodynamic properties of skutterudite (nominally $CoAs_3$)
84 and heazlewoodite (nominally Ni_3S_2). Enthalpies of formation were measured by high-
85 temperature oxide-melt solution calorimetry. The reference phases were pure elements, thus

eliminating potential systematic errors from reference chemical compounds. This work was also meant as another test of this type of calorimetry on samples with highly volatile components (As, S). Flushing with oxygen maintains oxidative conditions and all elements are converted rapidly and reproducibly to their highest oxidation state in the solvent (Majzlan 2017). The entropies were calculated from low-temperature heat capacities measured by relaxation calorimetry. Differential scanning calorimetry was used to measure C_p above the ambient temperature and the C_p data were extrapolated to higher temperatures using the appropriate treatment (Kieffer 1985). The data were then used to derive log K's for selected chemical reactions. These equilibrium constants can be used for geochemical modeling involving systems with Co-Ni sulfides and arsenides.

MATERIALS

The samples used in this study were prepared in evacuated silica tubes. The protocols described below are the results of many trials and errors, optimized to yield the desired products. Many other syntheses were carried out but did not run to completion, were contaminated by other minor sulfides/arsenides or oxygen.

A synthetic analog of heazlewoodite (Ni_3S_2) was prepared from a stoichiometric (3:2) mixture of pure elements (Ni 99.999 %, S 99.999 %) that were placed into a silica-glass tube. The tube with the charge was evacuated and sealed. The ampoule was placed into a preheated horizontal furnace, and the sample was tempered (200 °C for 32 days; 300 °C for 19 days). Afterwards, the sample was quenched in a cold-water bath, homogenized in an agate mortar, evacuated, sealed again, and heated (300 °C for two months). Finally, the sample was quenched, and the content purity and composition were checked using powder X-ray diffraction.

The synthetic analog of skutterudite was synthesized in evacuated silica-glass ampoules from pure elements (Co 99.9%, As 99.5%). The elements were weighed in an atomic ratio of 1:4 and placed in a silica-glass ampoule. The ampoule was evacuated, sealed and placed in a horizontal tube furnace. The temperature of that part of the ampoule, in which the charge was located, was 500 °C. The temperature of the opposite part was 450 °C. The synthesis lasted 50 days. The excess arsenic condensed in the colder part of the ampoule and was easily separated. After that the reacted mixture was removed, ground in an agate mortar under acetone, placed in another silica-glass ampoule, and heated at the same temperature for 30 days.

METHODS

Powder X-ray diffraction (PXRD) patterns of all compounds used in this work were collected using a Bruker D8 Advance DaVinci diffractometer (Institute of Geoscience of the University of Jena, Germany), employing Cu Kα radiation (λ = 1.54058 Å). The patterns were collected at room temperature between 5 and 90 º2θ, with a step size of 0.02 º2θ and a time per step of 1 s. Lattice parameters and quantitative fractions of the studied phases were refined by a full-profile fit using the software suite JANA2006 (Petříček et al., 2014).

The powdery synthetic phases were embedded in a resin and polished. They were briefly examined for impurity phases or inhomogeneities by reflected-light microscopy. The phases were investigated by energy- and wavelength-dispersive (WDX) electron microprobe (EMP) analyses with the electron microprobe JEOL JXA-8230 Superprobe (Institute of Geoscience of the University of Jena, Germany). All samples were carbon-coated and measured with an accelerating voltage of 20 kV and 20 nA. The spot size was 1 μm and the measurement time on peak and on background 40 s. Peak overlap correction was used to avoid peak interference between the lines of S and Co. The elements were analyzed on the following emission lines,

131 standards, with the estimated detection limits (in wt.%): Sb – Lα, InSb, 0.07; S – Kα, pyrite,
132 0.04; Fe – Kα, pyrite, 0.04; As – Kα, arsenopyrite, 0.07; Cu – Kα, chalcopyrite, 0.05; Co – Kα,
133 Co metal, 0.05; Ni – Kα, Ni metal, 0.04.

134 High-temperature oxide melt solution calorimetry has been described in detail by Navrotsky
135 (1997, 2014). The experiments were performed at the Arizona State University, USA. The
136 samples were dropped into a molten sodium molybdate ($3Na_2O \cdot 4MoO_3$) solvent, maintained at
137 1073 K. Oxygen gas was flushed over the solvent at 90 $mL \cdot min^{-1}$ and bubbled through it at 5
138 $mL \cdot min^{-1}$. The choice of the calorimetric solvents is limited to a few compositions, namely
139 sodium molybdate, lead borate, or alkali borate (see Navrotsky 1997). In the recent work of
140 Abramchuk et al. (2020), sodium molybdate at 1073 K was used to dissolve a suite of elements,
141 thus enabling to close the thermochemical cycle without the need for reference phases. We used
142 this advantage that also dictated the choice of the solvent and operation temperature.

143 Low temperature heat capacity (C_p) was measured by relaxation calorimetry using a
144 commercial Physical Properties Measurement System (PPMS, from Quantum Design, San
145 Diego, California) at the University of Salzburg, Austria. With due care, accuracy can be within
146 1 % at 5 K to 300 K, and 5 % at 0.7 K to 5 K (Dachs and Bertoldi, 2005; Kennedy et al., 2007).
147 The powdered samples were wrapped in a thin Al foil and compressed to produce a ≈0.5 mm
148 thick pellet, which was then placed onto the sample platform of the calorimeter for measurement.
149 Differential scanning calorimetry (DSC) was used to measure heat capacities near and above
150 room temperature using a Perkin Elmer Diamond DSC. Samples were measured in a flow of dry
151 argon. Further details of the method are described by Benisek et al. (2012). The entropy was
152 calculated by integration of the C_p/T function in the interval from 0 K to 298.15 K.

153 ## RESULTS

This is the peer-reviewed, final accepted version for American Mineralogist, published by the Mineralogical Society of America.
The published version is subject to change. Cite as Authors (Year) Title. American Mineralogist, in press.
DOI: https://doi.org/10.2138/am-2022-8337. http://www.minsocam.org/

Characterization: Powder X-ray diffraction, chemical analysis

All samples used in this study were crystalline and consisted of a single phase. No indications of an amorphous impurity were found. The peaks were sharp, with their width (measured as FWHM) comparable to that of the LaB_6 standard. Refined lattice parameters of all phases are given in Table 1. The PXRD patterns are shown in Figs. S1 and S2.

Examination with the electron microprobe confirmed that the samples consist of the elements of interest, either Ni-S or Co-As, with trace amount of other elements (Table 1). Images in back-scattered electrons (BSE) showed that the heazlewoodite and skutterudite samples were homogeneous. They were made of porous, angular aggregates, up to several hundreds of micrometers large, and their shape reflects the shape of the starting material (metal filing).

Chemical composition of the synthetic heazlewoodite sample corresponds to the nominal formula Ni_3S_2. For skutterudite, a slight deviation from the nominal formula was found. The composition, determined by EMP analyses, is $CoAs_{2.92}$. All thermodynamic data reported in this work are normalized to the molecular masses of Ni_3S_2 (240.2102 $g \cdot mol^{-1}$) and $CoAs_{2.92}$ (277.7043 $g \cdot mol^{-1}$).

Determination of enthalpies of formation

Enthalpies of formation were determined *via* appropriate thermochemical cycles (Tables 2, 3) from the experimentally measured drop solution enthalpies. No difficulties or anomalies were encountered during calorimetric experiments. The samples dissolved rapidly and reproducibly. The large drop solution enthalpies (Table 4) relate to the fact that the samples are oxidized and dissolved in the oxygen atmosphere in the active zone of the calorimeter. The large signals cause also larger uncertainties attached to the data; these uncertainties are expressed in calorimetry as

two standard deviations of the mean. Relative to the magnitude of the signal, the uncertainties are smaller than usually encountered. They are only 0.09 % and 0.24 % for the drop solution enthalpies of Ni_3S_2 and $CoAs_{2.92}$, respectively, which is smaller than the usual precision of 1-2 %. The resulting enthalpies of formation are given in Table 5.

Determination of low-temperature C_p and entropies

Heat capacity at temperatures between 2 and 303 K was measured for the synthetic heazlewoodite and skutterudite samples with the commercial PPMS system. The C_p data for both synthetic phases show no anomalies. Attempts to fit the low-temperature portion of the data ($T <$ 20 K) with a Debye function ($C_p = A_3T^3$) or an extended Debye function ($C_p = A_3T^3 + A_5T^5 + A_7T^7$) failed. Satisfactory fits required the inclusion of a linear (A_1T) or quadratic (A_2T^2) term, probably reflecting the semi-conducting nature of the phases studied (see Gopal 1966). The data between 20 and 300 K were fitted by two orthogonal polynomials. The adjustable parameters of these functions, together with the raw data and the results of integration, are available in the supporting electronic information. The calculated standard entropies (S^o at $T = 298.15$ K) are listed in Table 5.

Determination of high-temperature C_p

Heat capacity above 280 K was measured by differential scanning calorimetry (DSC). In the region of overlap of the DSC and PPMS data, the agreement between the data sets was good. The deviation was 1.3 % for heazlewoodite and 2.2 % for skutterudite. Upon increasing temperature, the data became unusually scattered. At $T \approx 366$ K (skutterudite) or ≈466 K (heazlewoodite), the data were so erratic that the measurements were stopped. Even though the samples were measured in an inert atmosphere of purified argon, it has to be assumed that traces

of oxygen caused partial oxidation of the samples. Of particular problem is sulfur or arsenic that co-exists in the gas phase with the studied phases (see Leegaard and Rosenqvist 1964). With increasing temperature, more sulfur or arsenic is transferred into the gas phase and can rapidly react with small amounts of oxygen.

Extrapolation of C_p up to 700 K

In order to be able to use the presented data for geochemical models of hydrothermal systems, heat capacity must be determined up to higher temperatures than those that were reached experimentally in this work. For this purpose, the available experimental C_p data were augmented by heat capacities at constant volume (C_v) computed using a model proposed by Kieffer (1985, her equation 60)

$$C_v \propto S(x_i) + K(x_u,x_i) + E(x_E) \qquad (7)$$

where $S(x_i)$ is the heat capacity function of a monatomic solid with a sine dispersion function, $K(x_u,x_i)$ refers to heat capacity of a continuum between frequencies x_u and x_i, and $E(x_E)$ is the heat capacity function of an Einstein oscillator. These functions and their prefactors are in detail defined by the equations 57-60 in Kieffer (1985) and will not be repeated here.

The frequencies necessary to calculate C_v according to (7) can be determined experimentally or by a lattice-dynamic calculation. We emphasize that the function (7) is not a fit to data but is based purely on experimental or calculated frequencies of low- to high-frequency modes in a structure. The function (7), as used in this work, contains no adjustable parameters.

For the calculation for skutterudite, frequencies of the Raman bands were taken from https://rruff.info/Skutterudite/R050593 (accessed on September 10, 2021). The frequencies for the acoustic branches were taken from Li and Mingo (2014) who performed first-principles calculations for the lattice dynamics of $CoSb_3$ skutterudite. For heazlewoodite, the Raman

222 frequencies were taken from https://rruff.info/Heazlewoodite (accessed on September 10, 2021).
223 The acoustic modes were characterized by first-principles calculations by Tian et al. (2021).

224 The isochoric heat capacity C_v can be used to calculate the isobaric heat capacity C_p as

225 $$C_p = C_v + VT\alpha^2B\kappa \qquad (8)$$

226 where V is the molar volume, T is the thermodynamic temperature, α is thermal expansion
227 coefficient, and B is the bulk modulus. The variable κ is the only adjustable parameter that enters
228 the calculations. It is necessary, because the calculated C_p is slightly lower than the experimental
229 C_p data. Such situation can be encountered in these calculations and is corrected by κ that can be
230 regarded as an anharmonicity term in the equation (8).

231 For skutterudite, α was taken from Rogl et al. (2010) for $CoSb_3$ skutterudite, and B from
232 Zouablia et al. (2020) for CoP_3 skutterudite. The value of κ was set to 2.4. For heazlewoodite, α
233 was taken from Tian et al. (2021), B from Zhang et al. (2020), and κ was set to 2.4.

234 The fits are compared to the experimental data and the extrapolations are shown in Fig. 1. The
235 results in the range of 280-700 K were re-fitted with polynomials accepted by the program
236 SUPCRTBL (Johnson et al. 1992, Zimmer et al. 2016):

237 $$C_p = a + bT + cT^{-2} + dT^{-0.5} \qquad (9)$$

238 The coefficients *a*-*d* are listed in Table 6 in the format required by SUPCRTBL. Note that the
239 values for the coefficients *a*, *c*, and *d* are to be used in SUPCRTBL as listed; the value of *b*
240 should be multiplied by 10^{-5} before inserting into the equation (9). The resulting C_p is in kJ·mol^{-1}·K^{-1}.

242 **DISCUSSION**

This is the peer-reviewed, final accepted version for American Mineralogist, published by the Mineralogical Society of America.
The published version is subject to change. Cite as Authors (Year) Title. American Mineralogist, in press.
DOI: https://doi.org/10.2138/am-2022-8337. http://www.minsocam.org/

Comparison of the data for heazlewoodite with earlier data

The enthalpies of formation of the two phases studied here can be compared to some previous results. The $\Delta_f H^o$ value for heazlewoodite (Table 5) is in excellent agreement with the value selected by Gamsjäger et al. (2005), based on the calorimetric work of Cemic and Kleppa (1986). They used reaction calorimetry with Ni+NiS mixtures sealed in evacuated silica tubes. The entropy of heazlewoodite, derived in this work, is also in excellent agreement with the selection of Gamsjäger et al. (2005). Our value is essentially identical with that from Weller and Kelley (1964) and only slightly higher than that from Stølen et al. (1991) (Table 5).

The perfect agreement for heazlewoodite confirms the accuracy of the data for the reference compounds and the applicability of high-temperature oxide-melt solution calorimetry. It lends support for the data for skutterudite where earlier data are missing.

Equilibria between nickel sulfides

The accuracy of the data for the nickel sulfides can be, to some extent, tested by comparison to known phase diagrams, as already presented in Gamsjäger et al. (2005). Sulfur pressure over nickel sulfide and the T-P(S_2,g) data were collected by Rosenqvist (1954) and Leegaard and Rosenqvist (1964). The pair heazlewoodite-millerite (β-NiS) is related by a simple reaction

$$2Ni_3S_2 + S_2(g) = 6\beta\text{-}NiS \qquad (10)$$

The data for millerite were taken from Gamsjäger et al. (2005). The log K_{10} values calculated with SUPCRTBL and the resulting sulfur gas fugacities are compared to the measured data in Fig. 2. The temperature ranges of the calculations and measurements do not overlap but linear extrapolation is possible. The difference between the log fS_2 values predicted with our data and

those from Rosenqvist (1954) (Fig. 2) at T = 900 K is ≈1.5, corresponding to $RT\Delta\ln fS_2$ of ≈26 kJ·mol^{-1}. Optimization of the data to fit the high-temperature measurements of Rosenqvist (1954) would be misleading because the nickel sulfides tend to non-stoichiometry at high temperatures (as $Ni_3S_{2\pm x}$, NiS_{1+x}, see Leegaard and Rosenqvist 1964). The deviation from stoichiometry is perhaps responsible for the mismatch seen in Fig. 2. Additionally, these phases have high-temperature polymorphs with slightly different thermodynamic properties (see Gamsjäger et al. 2005). All in all, the result of this test is encouraging for the accuracy of the data for heazlewoodite and millerite. More detailed calculation of the sulfur pressures in nickel-sulfide equilibria is provided by Gamsjäger et al. (2005) (their figure V-32) at high temperatures.

No attempt was made to incorporate the thermodynamic data for vaesite (NiS_2) into these calculations, even though Chase (1998) and Gamsjäger et al. (2005) list data for this phase. These data, however, are associated with unusually large uncertainties. They indicate another, underlying problem with these data. As a side note, we attempted to synthesize vaesite also for this study. The sample turned out to be a mixture of NiS_2 and Ni_3S_4. These two phases should have pyrite-like and spinel-like structures, respectively. Powder XRD data for our sample show only pyrite-like structure. This puzzling structural relationship will be more closely investigated but could be potentially a reason (or one of the reasons) for the problems related to the measurements on vaesite. Finally, the database Thermoddem (Blanc et al. 2012) contains temperature-dependent log K values for a dissolution reaction involving vaesite. Yet, a closer look at the values in this database (https://thermoddem.brgm.fr/species/nis2, accessed on September 9, 2021) shows that C_p of vaesite was taken as a constant over 0-300 °C. Such treatment of thermodynamic data is highly misleading and should be avoided.

Equilibrium constants for dissolution reactions

This is the peer-reviewed, final accepted version for American Mineralogist, published by the Mineralogical Society of America.
The published version is subject to change. Cite as Authors (Year) Title. American Mineralogist, in press.
DOI: https://doi.org/10.2138/am-2022-8337. http://www.minsocam.org/

Geochemical software used for modeling of aqueous solutions, either around room temperature or at elevated temperatures, commonly requires tabulation of equilibrium constants for selected dissolution reactions involving the phase of interest. For this purpose, all data presented above were inserted into SUPCRTBL (Zimmer et al. 2016) and the equilibrium constants were calculated.

The calculations are slightly complicated by the fact that the nominal valences, calculated from the formulae, differ from the valences usually assigned to the participating elements (such as Ni^{2+}, S^{2-}, and so on). For heazlewoodite, the reactions to consider are

$$Ni_3S_2(cr) + 6H^+(aq) + 0.5O_2(aq) \rightarrow 3Ni^{2+}(aq) + 2H_2S^0(aq) + H_2O(l) \quad (11)$$

$$Ni_3S_2(cr) + 4H^+(aq) + 0.5O_2(aq) \rightarrow 3Ni^{2+}(aq) + 2HS^-(aq) + H_2O(l) \quad (12)$$

Under most hydrothermal conditions, the aqueous species H_2S^0 will predominate over HS^-. The aggregate state of O_2 and H_2O is important inasmuch the software packages usually do not explicitly specify it for the master O_2 and H_2O species. The values of log K_{11} and log K_{12} in the temperature range 0-350 ºC are listed in Table S1.

For skutterudite, the oxidation reactions are

$$CoAs_{2.92}(cr) + 3.38H_2O(l) + 2.69O_2(aq) + 2H^+(aq) \rightarrow Co^{2+}(aq) + 2.92As(OH)_3^0(aq) \quad (13)$$

$$CoAs_{2.92}(cr) + 3.38H_2O(l) + 2.69O_2(aq) \rightarrow Co^{2+}(aq) + 2.92H_2AsO_3^-(aq) + 0.92H^+(aq) \quad (14)$$

For the arsenical species, $As(OH)_3^0$ is prevalent in hydrothermal fluids, and $AsO(OH)_2^-$ (this species is listed as $H_2AsO_3^-$ in GWB or AsO_2^- in SUPCRTBL) is subordinate, predominant only at pH > 8 at T = 300 ºC (Testemale et al. 2011). The values of log K_{13} and log K_{14} in the temperature range 0-350 ºC are listed in Table S1.

This is the peer-reviewed, final accepted version for American Mineralogist, published by the Mineralogical Society of America.
The published version is subject to change. Cite as Authors (Year) Title. American Mineralogist, in press.
DOI: https://doi.org/10.2138/am-2022-8337. http://www.minsocam.org/

Some geochemical software accepts a function that expresses log K in terms of absolute temperature T in Kelvin instead of log K values at a pre-selected temperature grid. PHREEQC, for example, uses the function in its **-analytic** option

$$\log K = A_1 + A_2T + A_3/T + A_4 \log T + A_5/T^2 \qquad (15)$$

GWB expresses the temperature dependence of log K as

$$\log K = a + b(T-T_r) + c(T^2-T_r^2) + d(1/T-1/T_r) + e(1/T^2-1/T_r^2) + f \ln(T/T_r) \qquad (16)$$

where T is absolute temperature in Kelvin and T_r = 298.15 K.

The fit parameters A_1-A_5 for equation (15) and the reactions (11) through (14) are listed in Table S2. The fit parameters a-f for equation (16) and the reactions (11) through (14) are listed in Table S3.

Relationship of skutterudite to other cobalt arsenides

The Δ_fH^o value for skutterudite (Table 5) can be only compared to an estimate which is significantly different. We are not aware of thermodynamic measurements on skutterudite.

The GWB and LLNL databases contain log K values for reactions involving safflorite ($CoAs_2$) and modderite (CoAs), even though no references are given. The log $K_{T=298.15}$ values match those given in Charykova et al. (2011) who also gave no references. Wagman et al. (1982) listed only Δ_fH^o for these phases, also without references. For example, they gave –61.5 kJ·mol^{-1} for $CoAs_2$, but Naumov et al. (1974) selected –83 kJ·mol^{-1}. These data, even though of uncertain origin, allow the calculation of phase diagrams whose informative value should not be overrated. Scharrer et al. (2019) constructed elaborate models with these phases and generated estimates for the missing data. Ironically, they themselves do not recommend the use of some of the data they

published (see their Table 3). We refrain from such practice and hold the opinion that geochemical modeling should be based on sound data. As pointed out by Henke (2009, appendix C) with respect to thermodynamics of arsenical phases, "once high-quality laboratory data are available, they may be used in geochemical computer models ...".

IMPLICATIONS

This work enhances the capabilities of geochemical modeling of hydrothermal ores, especially those of the so-called 'five-element association' (e.g., Kreissl et al. 2018, Scharrer et al. 2019, Horn et al. 2021, Tourner et al. 2021). Skutterudite is one of the major sources of cobalt in these ores, being used for the construction of lithium-ion batteries (Li et al. 2018). Therefore, understanding of these ores, the ore-forming processes, and identification of new resources is an important future task for the geosciences. This work also documented the capability of calorimetric techniques to obtain highly accurate data for chalcogenides. Combination of the experimental data with the Kieffer model generated accurate representation of high-temperature heat capacities and can be used to circumvent experimental difficulties associated with the measurements at high temperatures. This approach can be used to resolve some long-standing controversies in the thermodynamic data sets for common and less common chalcogenide minerals.

ACKNOWLEDGEMENTS

We are thankful to Valentina L. Stolyarova and Gleb Pokrovski for their constructive criticism and comments. The work presented here was financially supported by a *Deutsche Forschungsgemeinschaft* grant MA 3927/32-1. Oxide melt solution calorimetry was supported

by the U.S. Department of Energy Office of Basic Energy Sciences, under grant DE-FG02-97ER14749. The work of DACh is supported by RFBR, № 20-35-70049.

352 ## REFERENCES

353 Abramchuk, M., Lilova, K., Subramani, T., Yoo, R., and Navrotsky, A. (2020) Development of
354 high-temperature oxide melt solution calorimetry for p-block element containing materials.
355 Journal of Materials Research, 35, 2239.
356 Ahmed, A.H., Arai, S., and Ikenne, M. (2009) Mineralogy and paragenesis of the Co-Ni arsenide
357 ores of Bou Azzer, Anti-Atlas, Morocco. Economic Geology, 104, 249-266.
358 Barton, P.B. Jr. (1969) Thermochemical study of the system Fe-As-S. Geochimica et
359 Cosmochimica Acta 33, 841-867.
360 Bayliss, P., and Stephenson, N.C. (1967) The crystal structure of gersdorffite. Mineralogical
361 Magazine, 36, 38-42.
362 Bayliss, P., and Stephenson, N.C. (1968) The crystal structure of gersdorffite (III), a distorted
363 and disordered pyrite structure. Mineralogical Magazine, 36, 940-947.
364 Bayliss, P. (1982) A further crystal structure refinement of gersdorffite. American Mineralogist,
365 67, 1058-1064.
366 Belkin, H.E., and Luo, K. (2008) Late-stage sulfides and sulfarsenides in Lower Cambrian black
367 shale (stone coal) from the Huangjiawan mine, Guizhou Province, People's Republic of
368 China. Mineralogy and Petrology, 92, 321-340.
369 Benisek, A., Kroll, H., and Dachs, E. (2012) The heat capacity of fayalite at high temperatures.
370 American Mineralogist, 97, 657-660.
371 Bessinger, B., and Apps, J.A. (2005) The hydrothermal chemistry of gold, arsenic, antimony,
372 mercury and silver. U.S. Department of Energy, Contract No. DE-AC03-76SF00098, 52 p.
373 Blanc, P., Lassin, A., Piantone, P., Azaroual, M., Jacquemet, N., Fabbri, A., and Gaucher, E.C.,
374 (2012) Thermoddem: A geochemical database focused on low temperature water/rock
375 interactions and waste materials: Applied Geochemistry, 27, 2107-2116.
376 Burisch, M., Gerdes, A., Walter, B.F., Neumann, U., Fettel, M., and Markl, G. (2017) Methane
377 and the origin of five-element veins: Mineralogy, age, fluid inclusion chemistry and ore
378 forming processes in the Odenwald, SW Germany. Ore Geology Reviews, 81, 42-61.
379 Cabri, L.J., Kelvin, M., Yang, Z., Jackson, S.E., and Altun, O. (2017) Application of LA-ICP-
380 MS trace element analysis for precious metal deportment: A case study of the Kevitsa mine,
381 Finland. European Journal of Mineralogy, 29, 635-644.
382 Cemic, L., and Kleppa, O.J. (1986) High temperature calorimetry of sulfide systems. I.
383 Thermochemistry of liquid and solid phases of Ni+S. Geochimica et Cosmochimica Acta, 50,
384 1633-1641.
385 Charykova, M.V., Krivovichev, V.G., Yakovenko, O.S., and Depmeier, W. (2011)
386 Thermodynamics of arsenates, selenites, and sulfates in the oxidation zone of sulfide ores:
387 Part III: Eh–pH diagrams of the Me–As–H_2O systems (Me = Co, Ni, Fe, Cu, Zn, Pb) at 25°C.
388 Geology of Ore Deposits, 53, 501–513.
389 Chase, M.W. (1998) NIST-JANAF Thermochemical Tables. National Institute of Standards and
390 Technology, Gaithersburg (Maryland, USA).
391 Dachs, E., and Bertoldi, C. (2005) Precision and accuracy of the heat-pulse calorimetric
392 technique: low-temperature heat capacities of milligram-sized synthetic mineral samples.
393 European Journal of Mineralogy, 17, 251-261.
394 Dewaele, S., Muchez, Ph., Vets, J., Fernandez-Alonzo, M., and Tack, L. (2006) Multiphase
395 origin of the Cu–Co ore deposits in the western part of the Lufilian fold-and-thrust belt,
396 Katanga (Democratic Republic of Congo). Journal of African Earth Sciences, 46, 455-469.

Dolansky, L.L. (2007) Controls on the genesis of hydrothermal cobalt mineralization: Insights from the mineralogy and geochemistry of the Bou Azzer deposits, Morocco. Master thesis, McGill Univ., 193 p.

Gamsjäger, H., Bugajski, J., Gajda, T., Lemire, R., and Preis, W. (2005) Chemical Thermodynamics of Nickel. Volume 6, 1st Edition.

Gervilla, F., Fanlo, I., Colás, V., and Subías, I. (2012) Mineral compositions and phase relations of Ni-Co-Fe arsenide ores from the Aghbar mine, Bou Azzer, Morocco. Canadian Mineralogist, 50, 447-470.

Gonzáles-Jiménez, J., Pina, R., Saunders, J.E., Plissart, G., Marchesi, C., Padrón-Navarta J.A., Ramón-Fernandez, M., Garrido, L.N.F., and Gervilla, F. (2021) Trace element fingerprints of Ni–Fe–S–As minerals in subduction channel serpentinites. Lithos, 400-401, 106432, https://doi.org/10.1016/j.lithos.2021.106432

Gopal, E.S.R. (1966) Specific Heats at Low Temperatures. Plenum Press, New York.

Hayun, S., Lilova, K., Salhov, S., and Navrotsky, A. (2020) Enthalpies of formation of high entropy and multicomponent alloys using oxide melt solution calorimetry. Intermetallics, 125, 106897.

Hem, S.R., and Makovicky, E. (2004a) The system Fe–Co–Ni–As–S: I. Phase relations in the (Fe, Co, Ni)$As_{0.5}S_{1.5}$ section at 650 ºC and 500 ºC. Canadian Mineralogist, 42, 43-62.

Hem, S.R., and Makovicky, E. (2004b) The system Fe–Co–Ni–As–S: II. Phase relations in the (Fe, Co, Ni)$As_{1.5}S_{0.5}$ section at 650 ºC and 500 ºC. Canadian Mineralogist 42, 63-86.

Hem, S. (2006) Solid solutions in the Fe–Co–Ni–As–S system. Chemical Geology, 225, 291-303.

Henke, K.R. (editor) (2009) Arsenic. Environmental Chemistry, Health Threats and Waste Treatment. Wiley, 588 p.

Horn, S., Gunn, A.G., Petavratzi, E., Shaw, R.A., Eilu, P., Törmänen, T., Bjerkgård, T., Sandstad, J.S., Jonsson, E., Kountourelis, S., and Wall, F. (2021) Cobalt resources in Europe and the potential for new discoveries. Ore Geology Reviews, 130, 103915.

Johnson, J.W., Oelkers, E.H., and Helgeson, H.C. (1992) SUPCRT92 - A software package for calculating the standard molal thermodynamic properties of minerals, gases, aqueous species, and reactions from 1-bar to 5000-bar and 0°C to 1000°C. Computer and Geosciences, 18, 899-947.

Kennedy, C.A., Stancescu, M., Marriott, R.A., and White, M.A. (2007) Recommendations for accurate heat capacity measurements using a Quantum Design physical property measurement system. Cryogenics, 47, 107-112.

Kieffer, S.W. (1985) Heat capacity and entropy: systematic relations to lattice vibrations. Reviews of Mineralogy, 14, 65-126.

Klemm, D.D. (1965) Synthesen und analysen in den dreiecksdiagrammen FeAsS–CoAsS–NiAsS und FeS_2–CoS_2–NiS_2. Neues Jahrbuch für Mineralogie, Abhandlungen, 103, 205-255.

Kreissl, S., Gerdes, A., Walter, B.F., Neumann, U., Wenzel, T., and Markl, G. (2018) Reconstruction of a >200 Ma multi-stage "five element" Bi-Co-Ni-Fe-As-S system in the Penninic Alps, Switzerland. Ore Geology Reviews, 95, 746-788.

Leegaard, T., and Rosenqvist, T. (1964) Der Zersetzungsdruck und die Phasengleichgewichte der höheren Sulfide von Kobalt und Nickel. Zeitschrift für anorganische und allgemeine Chemie, 328, 294-298.

Li, W., and Mingo, N. (2014) Lattice dynamics and thermal conductivity of skutterudites $CoSb_3$ and $IrSb_3$ from first principles: Why $IrSb_3$ is a better thermal conductor than $CoSb_3$. Physical Review B, 90, 094302.

Li, M., Lu, J., Chen, Z., and Amine, K. (2018) 30 years of lithium-ion batteries. Advanced Materials, 30, 1800561, DOI: 10.1002/adma.201800561

Majzlan, J. (2017) Solution calorimetry on minerals related to acid mine drainage – methodology, checks, and balances. Acta Geologica Slovaca, 9, 171-183.

Maurel, C. and Picot, P. (1974) Stabilite de l'alloclasite et de la cobaltite dans le systeme Co–As–S et Co–Ni–As–S. Bulletin de la Societe Francaise de Minéralogie et de Cristallographie, 97, 251–256.

Naldrett, A.J. (2004) Magmatic Sulfide Deposits: Geology, Geochemistry and Exploration. Springer, 728 p.

Navrotsky, A. (1997) Progress and new directions in high temperature calorimetry revisited. Physics and Chemistry of Minerals, 24, 222-241.

Navrotsky, A. (2014) Progress and new directions in calorimetry: A 2014 perspective. Journal of the American Ceramic Society, 97, 3349-3359.

Naumov, G.B., Ryzhenko, B.N., and Khodakovsky, I.L. (1974) Handbook of Thermodynamic Data (English translation). USGS-WRD-74-001, U.S. Geological Survey.

Nordstrom, D.K., Königsberger, E., and Majzlan, J. (2014) Thermodynamic properties for arsenic minerals and aqueous species. Reviews in Mineralogy and Geochemistry 79, 217-255, doi.org/10.2138/rmg.2014.79.4

Pašava, J., Zaccarini, F., Aiglsperger, T., and Vymazalová, A. (2013) Platinum-group elements (PGE) and their principal carriers in metal-rich black shales: an overview with a new data from Mo–Ni–PGE black shales (Zunyi region, Guizhou Province, south China). Journal of Geosciences, 58, 209-216.

Pashinkin, A.C., Muratova, V.A., Moiseyev, N.V., and Bazhenov, J.V. (1991) Heat capacity and thermodynamic functions of iron diarsenide in the temperature range 5 K to 300 K. Journal of Chemical Thermodynamics, 23, 827-830.

Perfetti, E., Pokrovski, G.S., Ballerat-Busserolles, K., Majer, V., and Gibert, F. (2008) Densities and heat capacities of aqueous arsenious and arsenic acid solutions to 350 ^{o}C and 300 bar, and revised thermodynamic properties of $As(OH)_3^{o}$ (aq), $AsO(OH)_3^{o}$ (aq) and iron sulfarsenide minerals. Geochimica et Cosmochimica, Acta, 72, 713-731.

Petříček, V., Dušek, M., and Palatinus, L. (2014) Crystallographic computing system JANA2006: general features. Zeitschrift für Kristallographie, 229, 345–352. https://doi.org/10.1515/zkri-2014-1737

Pokrovski, G.S., Gout, R., Zotov, A., Schott, J., and Harrichoury, J.C. (1996) Thermodynamic properties and stoichiometry of the arsenic(III) hydroxide complexes at hydrothermal conditions. Geochimica et Cosmochimica Acta, 60, 737-749.

Pokrovski, G.S., Escoda, C., Blanchard, M., Testemale, D., Hazemann, J.-L., Gouy, S., Kokh, M.A., Boiron, M.-C., de Parseval, F., Aigouy, T., Menjot, L., de Parseval, P., Proux, O., Rovezzi, M., Béziat, D., Salvi, S., Kouzmanov, K., Bartsch, T., Pöttgen, R., and Doert, T. (2021) An arsenic-driven pump for invisible gold in hydrothermal systems. Geochemical Perspectives Letters, 17, 39–44, https://doi.org/10.7185/geochemlet.2112

Robie, R.A., and Hemingway, B.S. (1995) Thermodynamic properties of minerals and related substances at 298.15 K and 1 bar (10^5 Pascals) pressure and at higher temperatures. U.S. Geological Survey Bulletin, 2131, 461 p.

Rogl, G., Zhang, L., Rogl, P., Grytsiv, A., Falmbigl, M., Rajs, D., Kriegisch, M., Müller, H., Bauer, E., Koppensteiner, J., Schranz, W., Zehetbauer, M., Henkie, Z., and Maple, M.B. (2010) Thermal expansion of skutterudites. Journal of Applied Physics, 107, 043507.

Rosenqvist, T. (1954): A thermodynamic study of the iron, cobalt and nickel sulphides. Journal of Iron and Steel Institute, 176, 37-57.

Scharrer, M., Kreissl, S., and Markl, G. (2019) The mineralogical variability of hydrothermal native element-arsenide (five-element) associations and the role of physicochemical and kinetic factors concerning sulfur and arsenic. Ore Geology Reviews, 113, 103025. https://doi.org/10.1016/j.oregeorev.2019.103025

Steger, J., Nahigian, H., Arnott, R.J., and Wold, A. (1974) Preparation and characterisation of the solid solution series $Co_{1-x}Ni_xAsS$. Journal of Solid State Chemistry, 13, 53-59.

Števko, M., and Sejkora, J. (2020) Sb-enriched association of Ni arsenides and sulfarsenides from the Zemberg-Terézia vein system near Dobšiná (Western Carpathians, Slovak Republic). Bulletin Mineralogie Petrologie, 28, 105-115.

Stolyarova, T.A. (1977) Enthalpies of formation of iron arsenides. Geokhimia, 7, 1095-1098 (in Russian).

Stølen, S., Grønvold, F., Westrum, Jr., E.F., and Kolonin, G.R. (1991) Heat capacity and thermodynamic properties of synthetic heazlewoodite, Ni_3S_2, and of the high-temperature phase $Ni_{3\pm x}S_2$. Journal of Chemical Thermodynamics, 23, 77-93.

Takeno, N. (2005) Atlas of Eh-pH diagrams. Intercomparison of thermodynamic databases. Geological Survey of Japan Open File Report 419, 287 pp.

Tian, H., Liu, S., Zhang, Q., Zhao, Y., Tan, S., and Li, Y. (2021) First‐principles calculations of thermodynamic properties of Ni sulfides in the upper mantle. Physics and Chemistry of Minerals, 48, 30.

Testemale, D., Pokrovski, G.S. and Hazemann, J-L. (2011) Speciation of As^{III} and As^{V} in hydrothermal fluids by *in situ* X-ray absorption spectroscopy. European Journal of Mineralogy, 23, 379-390.

Tourneur, E., Chauvet, A., Kouzmanov, K., Tuduri, J., Paquez, C., Sizaret, S., Karfal, A., Moundi, Y., and El Hassani, A. (2021) Co-Ni-arsenide mineralisation in the Bou Azzer district (Anti-Atlas, Morocco): Genetic model and tectonic implications. Ore Geology Reviews, 134, 104128.

Wagman, D.D., Evans, W.H., Parker, V.B., Schumm, R.H., Halow, I., Bailey, S.M., Churney, K.L., and Nuttall, R.L. (1982) The NBS tables of chemical thermodynamic properties. Selected values for inorganic and C1 and C2 organic substances in SI units. Journal of Physical and Chemical Reference Data, 11, supplement 2.

Weller, W.W., and Kelley, K.K. (1964) Low-temperature heat capacities and entropies at 298.15 ^{o}K of sulfides of arsenic, germanium and nickel. Report of Investigations 6511, Department of the Interior, U.S.A.

Zhang, Q., Tian, Y., Liu, S., Yang, P., and Li, Y. (2020) First-principles study of the elastic properties of nickel sulfide minerals under high pressure. Minerals, 10, 737.

Zimmer, K., Zhang, Y.L., Lu, P., Chen, Y.Y., Zhang, G.R., Dalkilic, M., and Zhu, C. (2016) SUPCRTBL: A revised and extended thermodynamic dataset and software package of SUPCRT92. Computer and Geosciences, 90, 97-111. https://doi.org/10.1016/j.cageo.2016.02.013

Zouablia, R., Benabdellah, G., Mokhtari, M., and Hiadsi, S. (2020) Theoretical prediction of the structural, elastic, electronic and thermodynamic properties of binary CoP_3 and ternary

533 $FeCoP_3$ skutterudites materials. SPIN, 10, 2050011,
534 https://doi.org/10.1142/S2010324720500113
535
536
537

This is the peer-reviewed, final accepted version for American Mineralogist, published by the Mineralogical Society of America.
The published version is subject to change. Cite as Authors (Year) Title. American Mineralogist, in press.
DOI: https://doi.org/10.2138/am-2022-8337. http://www.minsocam.org/

Table 1. Space groups, lattice parameters (*a*, *c*, unit-cell volume *V*), and chemical composition (wt.%) of the synthetic phases used in this work. Chemical composition is recalculated to the molar ratio in the bottom part of the table. The numbers in parentheses are the uncertainties on the last significant digits.

nominal composition	Ni_3S_2	$CoAs_3$
actual composition	Ni_3S_2	$CoAs_{2.92}$
mineral name	heazlewoodite	skutterudite
space group	*R*32	*Im*-3
a (Å)	5.7476(1)	8.2050(2)
c (Å)	7.1397(1)	
n	13	11
Sb	< DL	< DL
S	26.83(28)	0.06(1)
As	0.04(6)	78.21(87)
Co	< DL	21.07(27)
Cu	< DL	< DL
Ni	72.65(40)	< DL
Fe	< DL	0.04(2)
total	99.54(38)	99.41(102)
	normalized to 1 Ni or Co atom	
S	0.676	
As		2.920
Co		1
Ni	1	

n = number of analyses averaged
< DL = below detection limit

Table 2. Thermodynamic cycle used to calculate the enthalpies of formation for heazlewoodite.

Ni_xS_y (s, 298 K) + $(2y+x/2)O_2$ (g, 1073 K) →	
xNi^{2+} (sol, 1073 K) + xO^{2-} (sol, 1073 K) + ySO_4^{2-} (sol, 1073 K)	ΔH_1
Ni (s, 298 K) + $0.5O_2$ (g, 1073 K) → Ni^{2+} (sol, 1073 K) + O^{2-} (sol, 1073 K)	ΔH_2
S (s, 298 K) + $2O_2$ (g, 1073 K) → SO_4^{2-} (sol, 1073 K)	ΔH_3
*x*Ni (s, 298 K) + *y*S (s, 298 K) → Ni_xS_y (s, 298 K)	$\Delta_fH^o = -\Delta H_1 + x\Delta H_2 + y\Delta H_3$

Table 3. Thermodynamic cycle used to calculate the enthalpy of formation for skutterudite.

$CoAs_z$ (s, 298 K) + $(2z+1/2)O_2$ (g, 1073 K) →	
Co^{2+} (sol, 1073 K) + O^{2-} (sol, 1073 K) + $zAsO_4^{3-}$ (sol, 1073 K)	ΔH_4
Co (s, 298 K) + $0.5O_2$ (g, 1073 K) → Co^{2+} (sol, 1073 K) + O^{2-} (sol, 1073 K)	ΔH_5
As (s, 298 K) + $2O_2$ (g, 1073 K) → AsO_4^{3-} (sol, 1073 K)	ΔH_6
Co (s, 298 K) + zAs (s, 298 K) → $CoAs_z$ (s, 298 K)	$\Delta_fH^o = -\Delta H_4 + \Delta H_5 + z\Delta H_6$

This is the peer-reviewed, final accepted version for American Mineralogist, published by the Mineralogical Society of America.
The published version is subject to change. Cite as Authors (Year) Title. American Mineralogist, in press.
DOI: https://doi.org/10.2138/am-2022-8337. http://www.minsocam.org/

Table 4. Drop solution enthalpies of the samples and reference phases. All values in $kJ \cdot mol^{-1}$.

samples	
Ni_3S_2	–1685.97[a]±1.56[b] (10)[c]
$CoAs_{2.92}$	–1424.46±3.40 (10)
reference phases	
Ni	–214.52±2.06 (Hayun et al. 2020)
Co	–227.75±2.18 (Hayun et al. 2020)
S	–629.18±2.73 (Abramchuk et al. 2020)
As	–440.03±1.57 (Abramchuk et al. 2020)

[a] mean
[b] two standard deviations of the mean
[c] number of measurements

Table 5. Summary of thermodynamic data for heazlewoodite and skutterudite, obtained in this work. Calculated enthalpies of formation are compared to the previously published literature values. Coefficients for the C_p polynomials are listed in Table 6.

	$\Delta_f H^o$ $kJ \cdot mol^{-1}$	S^o $J \cdot mol^{-1} \cdot K^{-1}$	$\Delta_f G^o$ $kJ \cdot mol^{-1}$	V^o $J \cdot bar^{-1}$
Ni_3S_2	–216.0±8.4	133.8±1.6	–210.0±8.4	4.095
	–217.2±1.6[a]	133.5±0.7[a]	–211.2±1.6[a]	
		133.89±0.84[b]		
		133.2[c]		
$CoAs_{2.92}$	–88.2±6.1	106.4±1.3	–79.9±6.2	4.159
	–104.6[d]			

[a] Gamsjäger et al. (2005)
[b] Weller and Kelley (1964)
[c] Stølen et al. (1991)
[d] theoretically calculated for $CoAs_3$, https://www.ctcms.nist.gov/~knc6/jsmol/JVASP-20306.html, accessed on July 21, 2021

Table 6. Adjustable coefficients for the C_p polynomial ($C_p = a + bT + cT^{-2} + dT^{-0.5}$, equation 9) for skutterudite and heazlewoodite. The numerical values are scaled as required by SUPCRTBL. See text for details.

phase	*a*	*b*	*c*	*d*
skutterudite	0.1096	0.8507	–535.1	–0.2695
heazlewoodite	0.1361	2.300	–872.4	–0.2490

This is the peer-reviewed, final accepted version for American Mineralogist, published by the Mineralogical Society of America.
The published version is subject to change. Cite as Authors (Year) Title. American Mineralogist, in press.
DOI: https://doi.org/10.2138/am-2022-8337. http://www.minsocam.org/

FIGURE CAPTIONS

Fig. 1. Experimental heat capacities from PPMS (circles) and DSC (squares) with the Kieffer model used to extrapolate C_p to higher temperatures. Note that this is not the fit used to determine entropy at T = 298.15 K.

Fig. 2. Equilibrium sulfur pressure for the pair heazlewoodite-millerite (reaction 10) calculated from the data presented and discussed in this work (diamonds) and experimentally measured by Rosenqvist (1954, circles). The linear fit is extrapolated to higher temperatures to allow for a visual judgment of the agreement between the two data sets.

This is the peer-reviewed, final accepted version for American Mineralogist, published by the Mineralogical Society of America.
The published version is subject to change. Cite as Authors (Year) Title. American Mineralogist, in press.
DOI: https://doi.org/10.2138/am-2022-8337. http://www.minsocam.org/

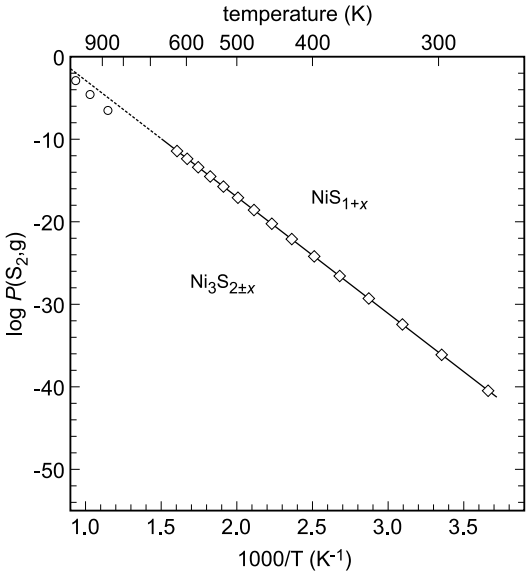

This is the peer-reviewed, final accepted version for American Mineralogist, published by the Mineralogical Society of America.
The published version is subject to change. Cite as Authors (Year) Title. American Mineralogist, in press.
DOI: https://doi.org/10.2138/am-2022-8337. http://www.minsocam.org/